Thermal characteristics of the phase transition near 100 K in $BaFe_2Al_9$

C. N. Kuo,[1,2] R. Y. Huang,[3] L. T. Wen,[1] H. Y. Lee,[4] C. K. Hong,[1] Y. R. Ou,[1,4] Y. K. Kuo,[3,*] and C. S. Lue[1,2,4,†]

[1]*Department of Physics, National Cheng Kung University, Tainan 70101, Taiwan*

[2]*Taiwan Consortium of Emergent Crystalline Materials, National Science and Technology Council, Taipei 10601, Taiwan*

[3]*Department of Physics, National Dong Hwa University, Hualien 97401, Taiwan*

[4]*Program on Key Materials, Academy of Innovative Semiconductor and Sustainable Manufacturing, National Cheng Kung University, Tainan 70101, Taiwan*

(Received 3 December 2023; revised 30 June 2024; accepted 2 July 2024; published 15 July 2024)

Novel intermetallic $BaFe_2Al_9$ has been of current interest due to indications of the charge-density wave (CDW) behavior associated with the structural phase transition. To further shed light on the nature of the phase transition, we carried out a detailed study by means of the specific-heat and thermoelectric measurements on single-crystalline specimens, mainly focusing on the signatures around the transition temperature $T_C \simeq 100$ K. For comparison, we investigated the isostructural compounds of $BaCo_2Al_9$ and $SrCo_2Al_9$, which showed no indications of the phase transition. While the measured physical quantities in both cobalt-based aluminides varied smoothly with temperature, those in $BaFe_2Al_9$ exhibited profound features with noticeable thermal hysteretic behavior in the vicinity of T_C. Based on the observed sudden enhancement in the Seebeck coefficient below T_C, we provide evidence for a decreased contribution from the *n*-type carriers undergoing the phase transition. The analysis of the thermal conductivity further indicated that both electronic and phononic origins were responsible for the drastic reduction in the observed thermal conductivity at T_C. We thus highlighted that the strong interplay between electronic and structural degrees of freedom gave rise to the peculiar phase transition in $BaFe_2Al_9$. Moreover, we compared the observed signatures with those reported in various CDW systems, and revealed important aspects of the emergence of CDW behavior in $BaFe_2Al_9$.

DOI: 10.1103/PhysRevB.110.045128

I. INTRODUCTION

Among the ternary aluminides with a three-dimensional (3D) hexagonal $BaFe_2Al_9$-type structure, only $BaFe_2Al_9$ exhibits a structural phase transition at the transition temperature $T_C \simeq 100$ K. [1]. The structural transition is intrinsically associated with discontinuous changes in the lattice parameters of about 0.5% increase in *a* and 1.5% shrinkage in *c*, a typical first-order phase transition in nature. Such an anisotropic distortion produces substantial mechanical strain, which results in the shattering of a chunk of crystal during the phase transition. The investigation of single-crystal x-ray-diffraction (XRD) measurement of the system revealed additional superlattice peaks below T_C, signifying the existence of the spatial modulation undergoing the phase transition. Further, refinement of the neutron-diffraction data at 70 K indicated that the observation was attributed to the modulated displacements at iron along the *c* axis and barium atoms in the *ab* plane. The large Fe atomic distortions have been suggested as the direction of the wave vector arising from charge-density wave (CDW) ordering [1]. Very recently, the nuclear magnetic resonance (NMR) measurement further provided evidence for a decrease in the electronic density of states (DOS) across the phase transition, consistent with the common signature for the CDW formation [2].

The simultaneous emergence of the CDW behavior together with a first-order structural transition in $BaFe_2Al_9$ is reminiscent of various 3D CDW systems, including the orthorhombic $U_2Co_3Si_5$-type $Lu_2Ir_3Si_5$ and $Er_2Ir_3Si_5$ [3–8], tetragonal $Sc_2Fe_3Si_5$-type $Sm_2Ru_3Ge_5$ and $Pr_2Ru_3Ge_5$ [9,10], and tetragonal $CaBe_2Ge_2$-type RPt_2Si_2 (*R*: rare-earth elements) [11–15]. It is worthwhile mentioning that the CDW mechanism in 3D structural materials is more complex than in the ideal 1D Peierls picture, where a nesting of Fermi surface (FS) in the electronic structure (i.e., formation of an energy gap) and a Kohn anomaly in phonon spectra occur simultaneously during the phase transition [16,17]. While the FS nesting may not necessarily take place in the 2D or 3D CDW systems, there could be imperfect nesting due to their anisotropic band structure and multicomponent FSs [17,18]. In addition, the *q*-dependent electron-phonon coupling and electron correlations play important roles for the CDW phase transition in these materials. For the present case of $BaFe_2Al_9$, incomplete FS nesting (i.e., partial gapping of FS) associated with the CDW ordering has been speculated [1]. Nevertheless, the proposed mechanisms responsible for the CDW formation remain unexplored.

In this study, a combination of specific-heat, electrical resistivity, Seebeck coefficient, and thermal conductivity measurements were carried out on single-crystalline $BaFe_2Al_9$. For comparison, we also performed the same measurements

*Contact author: ykkuo@mail.ndhu.edu.tw
†Contact author: cslue@mail.ncku.edu.tw

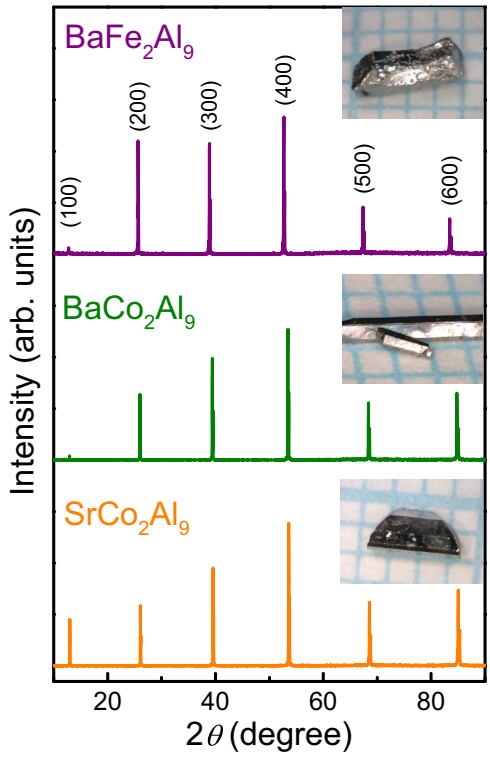

FIG. 1. Room-temperature single-crystal x-ray diffractions of the (00l) planes for $BaFe_2Al_9$, $BaCo_2Al_9$, and $SrCo_2Al_9$, respectively. All diffraction peaks can be indexed to the *P6/mmm* space group. Each inset shows a corresponding photograph of the crystal.

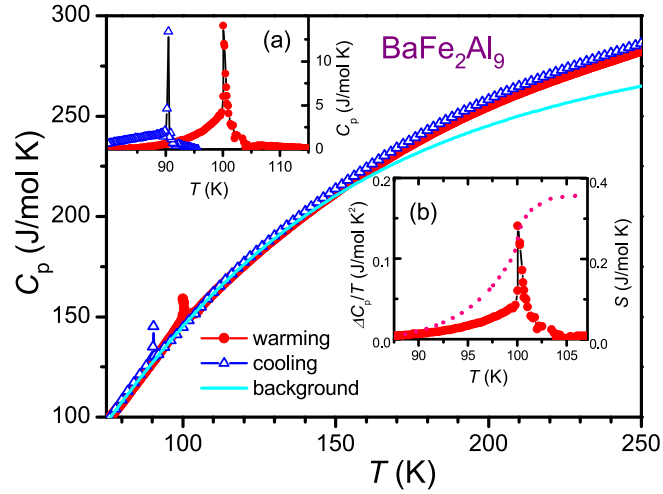

FIG. 2. Temperature dependence of the specific heat C_p for $BaFe_2Al_9$ and the background obtained by a combination of the Debye and Einstein models as discussed in the text. Inset (a) displays the excess specific heat ΔC_p for both cooling and warming processes. Inset (b) shows $\Delta C_p/T$ and the corresponding entropy S in the vicinity of T_C under a warming process.

on the sister compounds of $BaCo_2Al_9$ and $SrCo_2Al_9$, which did not indicate any phase transitions down to 4 K [1,19,20]. Distinctive features associated with thermal hysteresis in the vicinity of T_C were observed in $BaFe_2Al_9$ by all measured physical quantities. The analyses provided evidence that the phase transition involves a severe reconstruction of the electronic structures in addition to dramatic lattice distortions. Furthermore, the marked signatures near T_C were compared to those reported in various CDW materials, giving important viewpoints for the realization of the emergence of CDW behavior in $BaFe_2Al_9$.

II. EXPERIMENT AND DISCUSSION

Single crystals of $BaFe_2Al_9$, $BaCo_2Al_9$, and $SrCo_2Al_9$ were grown by using the Al self-flux method. For each individual material, the corresponding mixture of metallic elements was placed in an alumina crucible and sealed in a silica tube with partial argon. The ampoule was heated with a heating rate of 50 K/h to 1373 K and held at this temperature for 12 h, followed by cooling to 1173 K over 100 h. The remaining Al droplets on the crystal surfaces were etched in 1% HCl solution for 1 week. We thus obtained bulk crystals that exhibit a metallic luster, as shown in the inset of Fig. 1. The room-temperature single-crystal XRD patterns of each compound are displayed in Fig. 1, with the diffraction peaks indexed to the $BaFe_2Al_9$-type hexagonal structure (space group *P6/mmm*). We therefore determined the room-temperature lattice constants $a = 8.02$ Å and $c = 3.936$Å for $BaFe_2Al_9$; $a = 7.918$ Å and $c = 3.965$ Å for $BaCo_2Al_9$; and $a = 7.90$ Å and $c = 3.916$ Å for $SrCo_2Al_9$. These lattice parameters are close to those reported in the literature [1,2,19–21].

High-temperature specific-heat measurement was performed with a home-built ac calorimeter, employing chopped light as a heat source. While the ac technique has the advantage of high precision (∼1%), it only obtains the relative values of the specific heat. To get the absolute values, the specific-heat data here were normalized to the reported value at 200 K measured using a thermal relaxation technique [1]. Electrical resistivity data were obtained from a standard four-probe method, with electrical current flowing along the direction perpendicular to the c axis of the crystal. The Seebeck coefficient and thermal conductivity measurements were carried out in a closed-cycle refrigerator using a direct heat-pulse technique. The temperature difference was detected by an E-type differential thermocouple with junctions thermally attached to two well-separated positions along the longest direction of the specimen. To avoid microcracks or shattering of crystals caused by the strain during the structural phase transition in $BaFe_2Al_9$, we applied a slow scanning rate (<0.5 K/min) and used a small size of the specimen ($0.5 \times 0.4 \times 0.3\text{mm}^3$ for the electrical resistivity, $1.0 \times 0.5 \times 0.5\,\text{mm}^3$ for the Seebeck coefficient and thermal conductivity, and $0.5 \times 0.5 \times 0.1\text{mm}^3$ for the specific heat measurements). The uncertainty of electrical and thermal transport measurements is less than 15%, mainly arising from the error in the determination of the geometrical factor of the specimens.

Temperature dependence of the specific heat C_p between 80 and 300 K for $BaFe_2Al_9$ is shown in Fig. 2. Two spiky peaks at 90.5 and 100 K, measured during cooling and warming processes, respectively, are clearly discernible. The appearance of thermal hysteresis behavior demonstrates that the intrinsic phase transition is first order in nature. To elucidate

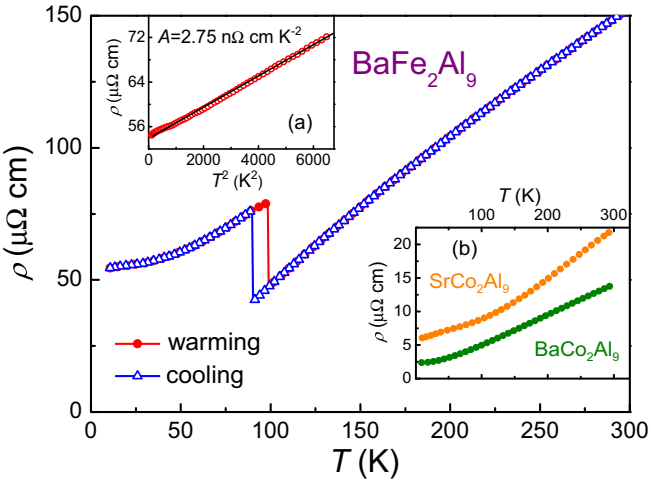

FIG. 3. Electrical resistivity ρ as a function of temperature for $BaFe_2Al_9$. Inset (a) displays a plot of ρ vs T^2, showing a linear relation below 80 K. The slope yields the temperature coefficient of the electric resistivity $A = 2.75\ \mathrm{n\Omega\,cm\,K^{-2}}$ obtained during a warming process. Inset (b) shows the temperature variations of ρ for $BaCo_2Al_9$ and $SrCo_2Al_9$, respectively.

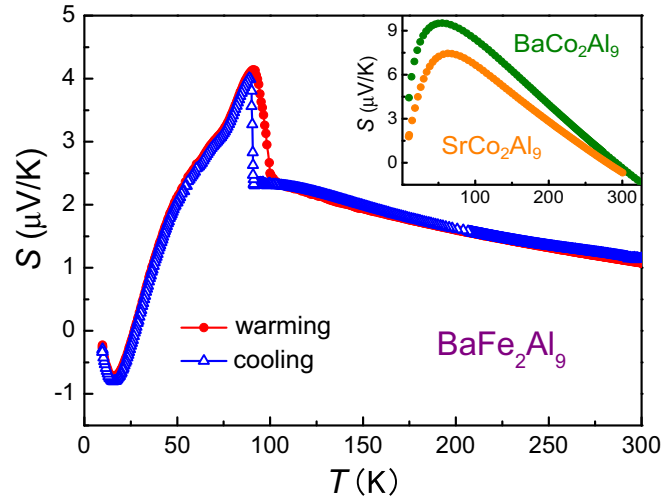

FIG. 4. Temperature dependence of the Seebeck coefficient S for $BaFe_2Al_9$. The inset shows the temperature variations of S for $BaCo_2Al_9$ and $SrCo_2Al_9$, respectively.

the thermodynamic characteristics of the phase transition, we analyzed the excess specific heat ΔC_p, obtained by subtracting a background of the specific heat, which was generated by a combination of Debye and Einstein models with a fixed value of electronic contribution (C_e), as reported previously [1]. The measured C_p data can be fitted up to 200 K by combining 92% Debye and 8% Einstein models with Debye temperature $\theta_D = 440$ K and Einstein temperature $\theta_E = 100$ K. These parameters, along with the dominant Debye model, are similar to those examined for $BaCo_2Al_9$ ($\theta_D = 398$ K and $\theta_E = 82$ K) and $SrCo_2Al_9$ ($\theta_D = 443$ K and $\theta_E = 99$ K) [19]. The upper inset of Fig. 2 displays the results of ΔC_p for both cooling and warming processes. It is worthwhile mentioning that the presence of a distinct ΔC_p with thermal hysteresis resembles those reported in the CDW compounds at the corresponding CDW ordering temperature. The examples include $Lu_2Ir_3Si_5$ [3], $Er_2Ir_3Si_5$ [8], $Pr_2Ru_3Ge_5$ [9], $PrPt_2Si_2$ [11], $EuAg_4As_2$ [22], $CaCu_4As_2$ [23], and the kagome metal ScV_6Sn_6 [24,25]. We also estimated the excess specific heat during the phase transition $\Delta C_p/C_p(T_C)$ of about 9% from the data measured under the warning process. To further evaluate the change in entropy ΔS associated with the phase transition, we first determined the temperature-dependent $\Delta C_p/T$ and then integrated $\Delta C_p/T$ through the entire phase-transition region. These results are illustrated in the lower inset of Fig. 2, revealing the magnitude of $\Delta S \simeq 0.36\mathrm{J\,mol^{-1}\,K^{-1}}$ for the phase transition of $BaFe_2Al_9$.

Temperature dependence of the electrical resistivity ρ for $BaFe_2Al_9$ is displayed in Fig. 3. The plot of the measured ρ for $BaCo_2Al_9$ and $SrCo_2Al_9$ is given in the lower inset of Fig. 3. Both cobalt-based aluminides exhibit typical metallic behavior with a positive temperature coefficient of the electrical resistivity, consistent with the previously observations [1,20]. For $BaFe_2Al_9$, the resistivity data below 80 K can be described well as a power law: $\rho(T) = \rho_0 + AT^2$, where ρ_0 is the residual resistivity mainly from scattering due to domain boundaries and defects by electrons and A is the temperature coefficient of the electric resistivity. In the upper inset of Fig. 3, we showed the plot of ρ vs T^2, with a linear relation yielding $\rho_0 = 53.9\,\mu\Omega$cm and $A = 2.75\mathrm{n\Omega cm\,K^{-2}}$. The characteristic of the T^2 term can be further related to the Sommerfeld coefficient for the electronic specific heat γ_e, expressed as the Kadowaki-Woods ratio A/γ_e^2, which is usually employed to examine the strength of the low-temperature electron-electron interaction of the studied system [26]. Taking the extracted $A = 0.00275$ $\mu\Omega\,\mathrm{cm\,K^{-2}}$ and $\gamma_e = 19.4\,\mathrm{mJ\,mol^{-1}\,K^{-2}}$ from the literature [1], we found $A/\gamma_e^2 = 0.73 \times 10^{-5}\ \mu\mathrm{W\,cm\,mol^2\,K^2\,mJ^{-2}}$ for $BaFe_2Al_9$. This value is close to the universal relation (10^{-5} $\mu\mathrm{W\,cm\,mol^2\,K^2\,mJ^{-2}}$) for the Fermi liquidlike systems [27], indicating the importance of the strong electron correlation in the low-temperature state of this material.

Upon cooling, ρ exhibits an abrupt upturn at 100 K with a thermal hysteresis width of about 10 K, identical to that reported by Meier *et al.* [1]. The observation is likely due to a partial gap in the FS of the band structure associated with the CDW formation. Nevertheless, the reduction in the carrier mobility caused by large strains during the structural phase transition is another possible mechanism responsible for the observed phenomenon. For further clarifying the true origin, more experiments, such as the analysis of the Hall coefficient measurement, is required. Here we estimated the resistivity jump at the phase transition $\Delta\rho/\rho(T_C) \simeq 66\%$ for $BaFe_2Al_9$. This value is comparable to those obtained in the CDW compounds of $Er_2Ir_3Si_5$ ($\simeq$62%) and $Ho_2Ir_3Si_5$ ($\simeq$ 82%) [8,28]. We also noticed that the features of the dramatic change in ρ and the spiky peak in C_p bear striking resemblances to those in $(Er, Ho)_2Ir_3Si_5$ [8,28]. The comparison implies similarities among the underlying mechanisms for the phase transition in these materials.

It is known that the Seebeck coefficient S is a sensitive probe for the phenomenon associated with changes in the FSs, such as CDW ordering and crystallographic distortion [4,29–47]. As shown in Fig. 4, the obtained S exhibits a

strong temperature dependence with a sign change below 30 K, indicative of the multi-band effect on the thermoelectric transport in $BaFe_2Al_9$. In the vicinity of T_C, a sudden change in S with noticeable thermal hysteresis behavior was observed. For the isostructural compounds of $BaCo_2Al_9$ and $SrCo_2Al_9$, the corresponding S is displayed in the inset of Fig. 4, showing a nearly identical temperature dependence with no change in the sign of S at low temperatures. For each material, the measured S increases monotonically with a broad maximum at around 70 K. The appearance of a hump feature is commonly seen in conventional metals at low temperatures, attributed to the phonon-drag effect arising from the umklapp phonon-phonon scattering process. Since the characteristic of S is strongly associated with the electronic structure of the studied material, the observations clearly indicate the intrinsic difference between the electronic structures of Fe- and Co-based aluminides. As a matter of fact, previous theoretical band-structure calculations revealed unfilled Fe d bands in $BaFe_2Al_9$ and filled Co d bands in $BaCo_2Al_9$ [1,20], being consistent with the present findings. In addition, the Sommerfeld electronic coefficient of $BaFe_2Al_9$ derived from low-temperature C_p data was approximately 4 times greater than those of the Co-based compounds [1]. It is worthwhile mentioning that the Hall measurement on the CDW compound of CsV_3Sb_5 suggested an interplay between electron mobility and hole concentration responsible for the change in the sign of S at low temperatures [48]. We thus speculate that the sign change in S is likely due to the interplay between scattering mechanisms and concentrations of different charge carriers in $BaFe_2Al_9$.

Since the measured S for $BaFe_2Al_9$ varies strongly with temperature, it can be appropriately described by a two-band model as $S = (\sigma_n S_n + \sigma_p S_p)/(\sigma_n + \sigma_p)$, where $S_{n,p}$ and $\sigma_{n,p}$ represent the Seebeck coefficients and electrical conductivities for the n- and p-type carriers from electronic and hole bands, respectively. In principle, each parameter is governed by the corresponding effective mass as well as the temperature-dependent scattering relaxation rate. Here, the positive sign of S indicates that the p-type carriers are predominant in the thermoelectric behavior. The drastic increase with lowering temperature below T_C can be realized as an imbalance of the contribution from different types of carriers induced by the phase transition. Accordingly, a reduced contribution from the n-type carriers would give rise to an enhancement in the observed S. Such an interpretation agrees with the previously theoretical model, where the filling of the Fe $3d$ orbitals by capturing the electrons from neighboring Al atoms plays an essential role in approaching the ground state of $BaFe_2Al_9$ [1]. It is also consistent with the NMR result, which revealed a reduction in the Al partial Fermi-level DOS below T_C [2]. A similar feature was noticed in the well-studied CDW compound of $SmNiC_2$, where the increase in S was ascribed to a substantial modification in the FS across the phase transition [45]. The comparison thus provides evidence for the DOS reduction along with the structure transition, which may lead to a CDW order in $BaFe_2Al_9$.

The main panel of Fig. 5 illustrates the temperature-dependent thermal conductivity κ for $BaFe_2Al_9$, showing an abrupt change with thermal hysteresis at T_C. In the inset of Fig. 5, we plotted κ as a function of temperature

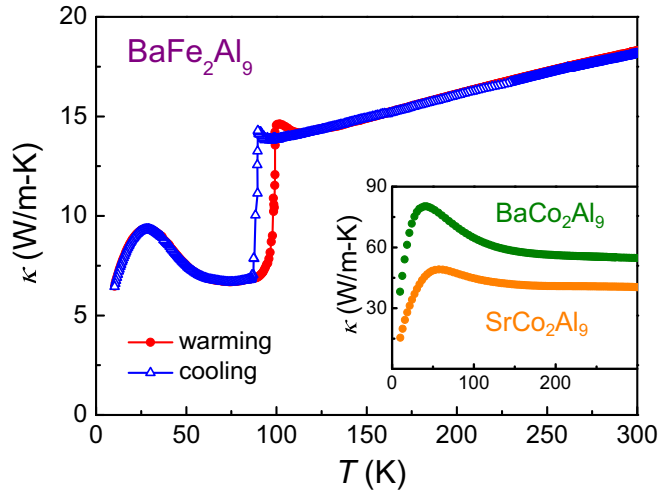

FIG. 5. Temperature dependence of the measured thermal conductivity κ for $BaFe_2Al_9$. The inset displays the temperature variations of κ for $BaCo_2Al_9$ and $SrCo_2Al_9$, respectively.

for both $BaCo_2Al_9$ and $SrCo_2Al_9$. At low temperatures, κ features a broad maximum at around 28, 40, and 55 K for $BaFe_2Al_9$, $BaCo_2Al_9$, and $SrCo_2Al_9$, respectively. The observation is likely caused by the reduction of the thermal scattering, and the maximum occurs at the temperature where the phonon mean-free path is approximately equal to the crystal site distance. In ordinary metals or semimetals, the measured κ is a sum of electronic and lattice contributions. The electronic thermal conductivity κ_e can be evaluated using the Wiedemann-Franz law: $\kappa_e \rho/T = L_0$, where $L_0 = 2.45 \times 10^{-8}\ \mathrm{W\,\Omega\,K^{-2}}$ is the theoretical Lorentz number and ρ is the experimental electrical resistivity. The lattice thermal conductivity κ_L was thus obtained by subtracting κ_e from the measured κ. The resolved κ_e and κ_L for the cooling process of $BaFe_2Al_9$ are depicted in Fig. 6. The same analysis was

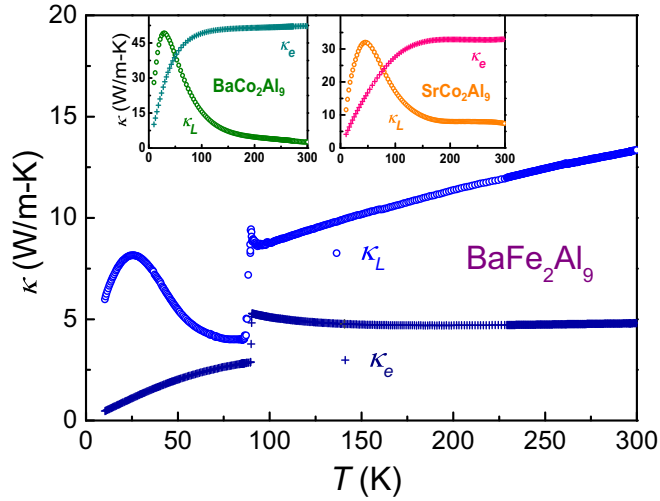

FIG. 6. Temperature variations of the electronic thermal conductivity κ_e and lattice thermal conductivity κ_L for $BaFe_2Al_9$ obtained during a cooling process. Each inset shows the decomposed κ_e and κ_L for $BaCo_2Al_9$ and $SrCo_2Al_9$, respectively.

employed on $BaCo_2Al_9$ and $SrCo_2Al_9$, with the results given in the insets of Fig. 6. For both cobalt-based aluminides, κ_e increases with temperature and becomes dominant at high temperatures. κ_L obeys a conventional $1/T$-type decrease with temperature, attributed to the umklapp phonon scattering process of the acoustic phonons.

For $BaFe_2Al_9$, $\kappa_e \simeq 4.8$ and $\kappa_L \simeq 13.3$ $W\,m^{-1}\,K^{-1}$ at room temperature were extracted. On this basis, we concluded that the thermal conductivity of $BaFe_2Al_9$ is mainly governed by κ_L at high temperatures. Remarkably, κ_L exhibits a glasslike linear increase instead of a crystalline monotonic decrease with temperature, similar to that observed in the CDW compounds of $Lu_5(Rh/Ir)_4Si_{10}$ and AV_3Sb_5 (A = K, Cs, and Rb) [29,46,49]. The exotic feature in κ_L was attributed to quasiparticle scattering resulting from charge fluctuations occurring along quasi-1D CDW chains via electron-phonon coupling. For the present case of $BaFe_2Al_9$, the characteristic of quasi-1D CDW with non-negligible fluctuations has been identified [1]. With this accordance, we pointed out that the linear temperature dependence of κ_L at high temperatures is a common signature for the chainlike CDW compounds with strong fluctuations and the presence of electron-phonon coupling in $BaFe_2Al_9$. While the exact strength of this coupling is unknown, it appears to play an essential role in the formation of CDW in the $BaFe_2Al_9$ system.

Another odd feature in κ_L is the appearance of a distinctive peak prior to T_C in $BaFe_2Al_9$. The corresponding excess lattice thermal conductivity $\Delta\kappa_L$ was found to be about 0.9 $W\,m^{-1}\,K^{-1}$, yielding the excess κ_L associated with the phase transition $\Delta\kappa_L/\kappa_L(T_C)$ of about 10%. Notably, this value is comparable to that of $Lu_5Ir_4Si_{10}$ ($\simeq$15%) [46]. The origin of large $\Delta\kappa_L$ in $Lu_5Ir_4Si_{10}$ was ascribed to the propagation of the softening phonon modes in the transition region, leading to considerable heat carried by the soft phonons. In this regard, one would expect a large number of soft phonons in the phonon-band dispersion of $BaFe_2Al_9$, which could enhance the electron-phonon coupling. The scenario drawn from the current investigation deserves further identification by means of theoretical calculations.

From the decomposed κ_e and κ_L in $BaFe_2Al_9$, we found that the drop in κ_e accounts for about 36% of the total thermal conductivity reduction at T_C. The substantial decrease in κ_e implies that the change in the electronic structure plays an important role in approaching the low-temperature ground state. The observation resembles those reported in $SmNiC_2$ and $Lu_5Ir_4Si_{10}$ [45,46]. The observed rapid drops in both materials are intrinsically caused by the reduction in κ_e with little contribution from κ_L, giving strong evidence for the electronic origin responsible for the CDW formation. Nevertheless, κ_L falls drastically at T_C, with a decrease of approximately 64% of the total reduction in $BaFe_2Al_9$. The dramatic change in κ_L is reminiscent of the signature in the materials with structural transformation [50,51]. The contribution from κ_L was connected to the change in the thermal diffusivity arising from different scattering of phonons undergoing the structural phase transition. In $BaFe_2Al_9$, a considerable anisotropic strain induced by the structural transformation would lead to a decrease in the thermal diffusivity and consequently lower the lattice thermal conductivity. Therefore, the current analysis of κ_e and κ_L near T_C gives an important viewpoint that the modification in both electronic and structural features plays an essential role in the peculiar phase transition in $BaFe_2Al_9$.

III. CONCLUSIONS

Thermal and transport properties at around T_C of $BaFe_2Al_9$ were characterized, revealing significant insights into the characteristics of the phase transition. In particular, we observed an enhancement in the Seebeck coefficient below T_C, which was accounted for by a decreased contribution from the n-type carriers due to a dramatic modification of electronic structures. We further demonstrated that both electronic and lattice thermal conductivities contribute to the drop of the total thermal conductivity undergoing the phase transition, indicating that the phase transition in $BaFe_2Al_9$ is not likely due to the purely electronic origin. Rather, the phonon-assisted enhancement in the lattice thermal conductivity during the structural phase transition is an important mechanism for the observation. With this accordance, we pointed out that the strong interplay between electronic and structural instabilities is a key factor responsible for the peculiar phase transition. In addition, we compared the signatures at around T_C to those reported in various CDW materials, yielding realistic viewpoints for the emergence of CDW behavior in $BaFe_2Al_9$.

ACKNOWLEDGMENTS

This work was supported by the National Science and Technology Council of Taiwan under Grants No. 112-2112-M-259-012, No. 111-2124-M-006-007, No. 112-2124-M-006-009, and No. 113-2112-M-006-024. The authors gratefully acknowledge Prof. Kuei Fang Hsu for the help in performing the single-crystal XRD measurement at the Core Facility Center of National Cheng Kung University under Grant No. 112-2740-M-006-001.

[1] W. R. Meier, B. C. Chakoumakos, S. Okamoto, M. A. McGuire, R. P. Hermann, G. D. Samolyuk, S. Gao, Q. Zhang, M. B. Stone, A. D. Christianson, and B. C. Sales, Chem. Mater. **33**, 2855 (2021).

[2] C. Y. Huang, H. Y. Lee, Y. C. Chang, Chon Kit Hong, Y. R. Ou, C. N. Kuo, and C. S. Lue, Phys. Rev. B **106**, 195101 (2022).

[3] Y. Singh, D. Pal, S. Ramakrishnan, A. M. Awasthi, and S. K. Malik, Phys. Rev. B **71**, 045109 (2005).

[4] Y. K. Kuo, K. M. Sivakumar, T. H. Su, and C. S. Lue, Phys. Rev. B **74**, 045115 (2006).

[5] M. H. Lee, C. H. Chen, M.-W. Chu, C. S. Lue, and Y. K. Kuo, Phys. Rev. B **83**, 155121 (2011).

[6] N. S. Sangeetha, A. Thamizhavel, C. V. Tomy, S. Basu, A. M. Awasthi, P. Rajak, S. Bhattacharyya, S. Ramakrishnan, and D. Pal, Phys. Rev. B **91**, 205131 (2015).

[7] S. Ramakrishnan, A. Schönleber, J.-K. Bao, T. Rekis, S. R. Kotla, A. M. Schaller, S. van Smaalen, L. Noohinejad,

M. Tolkiehn, C. Paulmann, N. S. Sangeetha, D. Pal, A. Thamizhavel, and S. Ramakrishnan, Phys. Rev. B **104**, 054116 (2021).

[8] S. Ramakrishnan, A. Schönleber, T. Rekis, N. van Well, L. Noohinejad, S. van Smaalen, M. Tolkiehn, C. Paulmann, B. Bag, A. Thamizhavel, D. Pal, and S. Ramakrishnan, Phys. Rev. B **101**, 060101(R) (2020).

[9] D. E. Bugaris, C. D. Malliakas, F. Han, N. P. Calta, M. Sturza, M. J. Krogstad, R. Osborn, S. Rosenkranz, J. P. C. Ruff, G. Trimarchi, S. L. Bud'ko, M. Balasubramanian, D. Y. Chung, and M. G. Kanatzidis, J. Am. Chem. Soc. **139**, 4130 (2017).

[10] D. E. Bugaris, C. D. Malliakas, S. L. Bud'ko, N. P. Calta, D. Y. Chung, and M. G. Kanatzidis, Inorg. Chem. **56**, 14584 (2017).

[11] M. Kumar, V. K. Anand, C. Geibel, M. Nicklas, and Z. Hossain, Phys. Rev. B **81**, 125107 (2010).

[12] Y. Nagano, N. Araoka, A. Mitsuda, H. Yayama, H. Wada, M. Ichihara, M. Isobe, and Y. Ueda, J. Phys. Soc. Jpn. **82**, 064715 (2013).

[13] R. Gupta, K. P. Rajeev, and Z. Hossain, J. Phys.: Condens. Matter **30**, 475603 (2018).

[14] M. Falkowski, P. Doležal, A. V. Andreev, E. Duverger-Nédellec, and L. Havela, Phys. Rev. B **100**, 064103 (2019).

[15] B. Shen, F. Du, R. Li, A. Thamizhavel, M. Smidman, Z. Y. Nie, S. S. Luo, T. Le, Z. Hossain, and H. Q. Yuan, Phys. Rev. B **101**, 144501 (2020).

[16] R. E. Peierls, *Quantum Theory of Solids* (Clarendon, Oxford, 1955).

[17] X. Zhu, Y. Cao, J. Zhang, E. W. Plummer, and J. Guo, Proc. Natl. Acad. Sci. USA **112**, 2367 (2015).

[18] X. Zhu, J. Guo, J. Zhang, and E. W. Plimmer, Adv. Phys.: X **2**, 622 (2017).

[19] Z. Ryzynska, T. Klimczuk, and M. J. Winiarski, J. Solid State Chem. **289**, 121509 (2020).

[20] C. Bigi, S. Pakdel, M. J. Winiarski, P. Orgiani, I. Vobornik, J. Fujii, G. Rossi, V. Polewczyk, P. D. C. King, G. Panaccione, T. Klimczuk, K. S. Thygesen, and F. Mazzola, Phys. Rev. B **108**, 075148 (2023).

[21] K. Turban and H. Schäfer, J. Less-Common Met. **40**, 91 (1975).

[22] B. Shen, C. Hu, H. Cao, X. Gui, E. Emmanouilidou, W. Xie, and N. Ni, Phys. Rev. Mater. **4**, 064419 (2020).

[23] S. Sasmal, V. Saini, S. Ramakrishnan, G. Dwari, B. B. Maity, J.-K. Bao, R. Mondal, V. Tripathi, S. van Smaalen, B. Singh, and A. Thamizhavel, Phys. Rev. Res. **4**, L012011 (2022).

[24] H. W. S. Arachchige, W. R. Meier, M. Marshall, T. Matsuoka, R. Xue, M. A. McGuire, R. P. Hermann, H. Cao, and D. Mandrus, Phys. Rev. Lett. **129**, 216402 (2022).

[25] Y. Hu, J. Ma, Y. Li, D. J. Gawryluk, T. Hu, J. Teyssier, V. Multian, Z. Yin, Y. Jiang, S. Xu, S. Shin, I. Plokhikh, X. Han, N. C. Plumb, Y. Liu, J. Yin, Z. Guguchia, Y. Zhao, A. P. Schnyder, X. Wu, E. Pomjakushina, M. Z. Hasan, N. Wang, and M. Shi, Nat. Commun. **15**, 1658 (2024).

[26] K. Kadowaki and S. B. Woods, Solid State Commun. **58**, 507 (1986).

[27] N. Tsujii, H. Kontani, and K. Yoshimura, Phys. Rev. Lett. **94**, 057201 (2005).

[28] S. Ramakrishnan, J. Bao, C. Eisele, B. Patra, M. Nohara, B. Bag, L. Noohinejad, M. Tolkiehn, C. Paulmann, A. M. Schaller, T. Rekis, S. R. Kotla, A. Schönleber, A. Thamizhavel, B. Singh, S. Ramakrishnan, and S. van Smaalen, Chem. Mater. **35**, 1980 (2023).

[29] C. S. Lue, Y. K. Kuo, F. H. Hsu, H. H. Li, H. D. Yang, P. S. Fodor, and L. E. Wenger, Phys. Rev. B **66**, 033101 (2002).

[30] A. T. Burkov, T. Nakama, M. Hedo, K. Shintani, K. Yagasaki, N. Matsumoto, and S. Nagata, Phys. Rev. B **61**, 10049 (2000).

[31] C. S. Lue, Y. F. Tao, K. M. Sivakumar, and Y. K. Kuo, J. Phys.: Condens. Matter **19**, 406230 (2007).

[32] E. D. Mun, S. L. Bud'ko, and P. C. Canfield, J. Phys.: Condens. Matter **23**, 476001 (2011).

[33] C. S. Lue, H. F. Liu, S. L. Hsu, M. W. Chu, H. Y. Liao, and Y. K. Kuo, Phys. Rev. B **85**, 205120 (2012).

[34] C. N. Kuo, H. F. Liu, C. S. Lue, L. M. Wang, C. C. Chen, and Y. K. Kuo, Phys. Rev. B **89**, 094520 (2014).

[35] Y. Liu, W. J. Lu, D. F. Shao, L. Zu, X. C. Kan, W. H. Song, and Y. P. Sun, EPL **109**, 17003 (2015).

[36] C. N. Kuo, C. W. Tseng, C. M. Wang, C. Y. Wang, Y. R. Chen, L. M. Wang, C. F. Lin, K. K. Wu, Y. K. Kuo, and C. S. Lue, Phys. Rev. B **91**, 165141 (2015).

[37] M. K. Hooda and C. S. Yadav, Appl. Phys. Lett. **111**, 053902 (2017).

[38] C. N. Kuo, W. T. Chen, C. W. Tseng, C. J. Hsu, R. Y. Huang, F. C. Chou, Y. K. Kuo, and C. S. Lue, Phys. Rev. B **97**, 094101 (2018).

[39] Y. Liu, H. Lei, K. Wang, M. Abeykoon, J. B. Warren, E. Bozin, and C. Petrovic, Phys. Rev. B **98**, 094519 (2018).

[40] C. N. Kuo, D. Shen, B. S. Li, N. N. Quyen, W. Y. Tzeng, C. W. Luo, L. M. Wang, Y. K. Kuo, and C. S. Lue, Phys. Rev. B **99**, 235121 (2019).

[41] M. K. Hooda, T. S. Tripathi, and C. S. Yadav, J. Alloys Compd. **785**, 603 (2019).

[42] C. N. Kuo, C. J. Hsu, C. W. Tseng, W. T. Chen, S. Y. Lin, W. Z. Liu, Y. K. Kuo, and C. S. Lue, Phys. Rev. B **101**, 155140 (2020).

[43] C. N. Kuo, R. Y. Huang, Y. K. Kuo, and C. S. Lue, Phys. Rev. B **102**, 155137 (2020).

[44] X. Mi, W. Xia, L. Zhang, Y. Gan, K. Yang, A. Wang, Y. Chai, Y. Guo, X. Zhou, and M. He, New J. Phys. **24**, 093021 (2022).

[45] J. H. Kim, J. S. Rhyee, and Y. S. Kwon, Phys. Rev. B **86**, 235101 (2012).

[46] Y. K. Kuo, C. S. Lue, F. H. Hsu, H. H. Li, and H. D. Yang, Phys. Rev. B **64**, 125124 (2001).

[47] R. Gumeniuk, K. O. Kvashnina, W. Schnelle, A. Leithe-Jasper, and Y. Grin, Phys. Rev. B **91**, 094110 (2015).

[48] Y. Gan, W. Xia, L. Zhang, K. Yang, X. Mi, A. Wang, Y. Chai, Y. Guo, X. Zhou, and M. He, Phys. Rev. B **104**, L180508 (2021).

[49] K. Yang, W. Xia, X. Mi, L. Zhang, Y. Gan, A. Wang, Y. Chai, X. Zhou, X. Yang, Y. Guo, and M. He, Phys. Rev. B **107**, 184506 (2023).

[50] C. S. Lue, Y.-K. Kuo, S.-N. Huang, S. Y. Peng, and C. Chen, Phys. Rev. B **71**, 064202 (2005).

[51] H. Chen, Z. Yue, D. Ren, H. Zeng, T. Wei, K. Zhao, R. Yang, P. Qiu, L. Chen, and X. Shi, Adv. Mater. **31**, 1806518 (2018).